

A finite volume method for scalar conservation laws with stochastic time-space dependent flux function

Kamel Mohamed^a, Mohammed Seaid^b, Mostafa Zahri^{c,*}

^a*Department of Computer Science, Faculty of Applied Sciences, University of Taibah Madinah, KSA*

^b*School of Engineering and Computing Sciences, University of Durham, South Road DH1 3LE, UK*

^c*Department of Mathematics, Faculty of Sciences, University of Taibah, P.O. Box 344 Madinah, KSA*

Abstract

We propose a new finite volume method for scalar conservation laws with stochastic time-space dependent flux function. The stochastic effects appear in the flux function and can be interpreted as a random manner to localize the discontinuity in the time-space dependent flux function. The location of the interface between the fluxes can be obtained by solving a system of stochastic differential equations for the velocity fluctuation and displacement variable. In this paper we develop a modified Rusanov method for the reconstruction of numerical fluxes in the finite volume discretization. To solve the system of stochastic differential equations for the interface we apply a second-order Runge-Kutta scheme. Numerical results are presented for stochastic problems in traffic flow and two-phase flow applications. It is found that the proposed finite volume method offers a robust and accurate approach for solving scalar conservation laws with stochastic time-space dependent flux functions.

Key words: Conservation laws, Stochastic differential equations, Finite volume method, Runge-Kutta scheme, Traffic flow, Buckley-Leverett equation

1 Introduction

Many practical problems in physics and engineering applications are modeled by conservation laws with time-space dependent flux function. These problems

* Corresponding author.

Email address: mzahri@taibahu.edu.sa (Mostafa Zahri).

have been extensively studied in the literature and their numerical solution can be accurately computed provided the flux functions, involved coefficients, initial and boundary data are given in a deterministic way. However, modeling realistic applications by conservation laws is complicated by the high heterogeneity of the involved coefficients combined with insufficient information characterizing the flux functions. For instance, in the simulation of transport models in ground water flows the exact knowledge of the permeability of the soil, the magnitude of source terms, inflow or outflow are usually not known, see [47] and further references are therein. Another example concerns the traffic flow in multi-lane roads where the behavior of drivers may turn to random in making the decision in which lane should the car be, see for example [46,3]. Other applications include multi-phase flow problems [18] conservation laws in networks [40] and production in supply chains [5]. For supply chains, the uncertainty is included in the processors as random breakdowns and random repair times. Under these circumstances the probabilistic aspects of the problem under consideration need to be taken into account for a realistic simulation of its numerical solution. The uncertainties mentioned above can be conveniently described by random fields, whose statistics are usually inferred from experiments. This requires to include, in the conservation laws modeling the problem at hands, a rational assessment of uncertainty, we refer the reader to [7,32,13,14,16] for more details on the uncertainty quantification in conservation laws. Consequently, this leads to the notion of scalar conservation laws with stochastic time-space dependent flux function. For the problems considered in this study, a stochastic differential system, for the velocity fluctuation and the displacement, is used to quantify uncertainties in the conservation laws. More precisely, the location of the discontinuity in the flux function is assumed to be driven by a drift towards the expected value and a stochastic noise term governed by the derivative of a Wiener process. In comparison with the deterministic conservation laws with discontinuous flux function, the appearance of the noise in the location of the interface can be seen as the integral effect of microscopic interactions, which produce a continuous sequence of small and almost stochastic velocity and location changes.

A number of numerical methods have been developed to solve stochastic partial differential equations. The obvious methods widely used in the literature are the Monte-Carlo algorithms. These methods generate a sequence of independent realizations of the solution by sampling the coefficients involved in the problem under consideration and solving the resulting deterministic partial differential equations using standard numerical tools. The obtained solutions are used to compute statistical characteristics of the solution in the problem, see [20] among others. However, Monte-Carlo algorithms are known to be computationally expensive and are only recommended as the last resort. Another method widely used in computational fluid dynamics is the Wiener chaos expansions, see for example [9,19]. In this approach, random fields are discretized using polynomial chaos resulting in a set of coupled deterministic partial differential equations to be solved for each chaos coefficient. However, the Wiener

chaos expansions have some limitations in application to the conservation laws with complex stochastic flux functions. For instance, large number of chaos coefficients in the expansions are needed to accurately compute small scales. In addition, many realizations have to be performed to obtain accurate estimates of the required statistical characteristics. Therefore, Wiener chaos expansions are computationally expensive. On the other hand, solving stochastic partial differential equations using properties of Wick calculus was also discussed, for instance in [17,29]. The main idea of this approach is to use properties of the Wick product along with the Hermite polynomials to decompose solution variables using an orthogonal basis and solve series of uncoupled deterministic equations. However, the treatment of nonlinear stochastic conservation laws in these methods is not trivial and high-order statistical moments are not easy to compute. The concept of incorporating uncertainty in linear hyperbolic equations of conservation laws is not new, see for example [49,43,11]. The mathematical equations studied in these references consist of the model scalar wave equation with random wave speed subject to given truncated Karhunen-Loève expansions. In addition, the numerical techniques presented in these references are essentially based on a spectral representation in random space that exhibits fast convergence only when the solution depends smoothly on the involved random parameters. On the other hand, there are several well-established techniques for modeling stochastic effects such as Galerkin projection, chaos polynomials, and collocation methods among others. Recently, the trend has focused on the development of numerical methods which model nonlinear hyperbolic systems of conservation laws. These include the incorporation of stochastic perturbations into the forcing terms [4], and the incorporation of stochastic variables into the physical flux functions [45,32]. The latter method has recently been extended by using adaptive anisotropic spectral procedures [44], such that the stochastic resolution level is based on the local smoothness of the solution in the stochastic domain. For the construction of numerical fluxes, the authors in [45,32,44] consider the Roe-type method which may become computationally expensive for hyperbolic systems of conservation laws with source terms and it may also require entropy correction to accurately capture shocks. Furthermore, truncation techniques in the polynomial chaos expansions may result in non-physical solutions such as negative second-order statistical moments. So the method of polynomial chaos expansions can be applied only for limited applications in nonlinear conservation laws. In the current work, we are interested in scalar conservation laws for which the physical flux function switches from one form to another depending on a random location in the spatial domain. This allows the flux function in the conservation laws under study to vary in the space and random variables. The location and speed of the discontinuity in the flux function are resolved by solving an extra system of stochastic ordinary differential equations. The aim of the present work is to implement a robust algorithm for solving scalar conservation laws with stochastic time-space dependent flux function. The key idea consists on combining a finite volume method for the spatial

discretization with a second-order explicit stochastic Runge-Kutta scheme developed in [35–37] for the time integration of the stochastic differential equations. The emphasis in this study is given to a modified Rusanov method studied and analyzed in [30] for the spatial discretization. This method is simple, accurate and avoids the solution of Riemann problems during the time integration process. The combined method is linearly stable provided the condition for the canonical Courant-Friedrichs-Lewy (CFL) condition is satisfied. Our main goal is to present a class of numerical methods that are simple, easy to implement, and accurately solves the stochastic conservation laws without relying on a Riemann solver or direct statistical algorithms. We should mention that the finite volume method presented in this paper also differs from the traditional Rusanov approach [38] in the fact that the characteristic speed is assumed to be constant, whereas in the present work we use an adaptive selection of the characteristic speed based on the location of shocks within the computational domain. To the best of our knowledge, this is the first time that a finite volume method is used to solve stochastic equations of nonlinear conservation laws with discontinuous time-space dependent flux functions.

Numerical results are illustrated for several test examples on scalar conservation laws with stochastic time-space dependent flux function. In the first case, analytical solution is available and thus it can be used for verification of convergence rates and accuracy of the proposed numerical schemes. In the other cases, comparison to deterministic solutions is presented to illustrate stochastic effects. Our method accurately approximates the numerical solution to these nonlinear problems. The obtained results demonstrate good shock resolution with high accuracy in smooth regions and without any nonphysical oscillations near the shock areas or extensive numerical dissipation. The performance of the developed solvers is very attractive since the computed solutions remain stable, monotone and highly accurate without solving Riemann problems or using demanding computational resources.

The rest of this paper is organized as follows. In section 2 we introduce the equations for scalar conservation laws with stochastic time-space dependent flux function. The finite volume method for stochastic conservation laws is formulated in section 3. This section also includes the time integration of the stochastic differential equations for the interface and the reconstruction of the numerical fluxes in the finite volume discretization. In section 4 we present numerical results for several test examples. Section 5 summarizes the paper with concluding remarks.

2 Stochastic conservation laws

Let $(\Omega, \mathcal{F}, \mathbb{P})$ be a probability space, where Ω is the space of basic outcomes, \mathcal{F} is the σ -algebra associated with Ω , and \mathbb{P} is the (probability) measure on \mathcal{F} . This σ -algebra can be interpreted as a collection of all possible events that could be derived from the basic outcomes in Ω , and that have a probability

that is well defined with respect to P . A random variable X is a mapping $X : \Omega \longrightarrow \mathbb{R}$. The L^p -norm of a random variable can be defined as

$$\|X\|_p = \langle |X|^p \rangle^{1/p}, \quad \text{for } 0 < p < \infty,$$

where $\langle \cdot \rangle$ denotes the operation of mathematical expectation. Equipped with this norm, the space L^p is a Banach space of all random variables X defined on (Ω, \mathcal{F}, P) and having a finite norm. In the current study, we are interested in developing robust numerical methods for approximating solutions of the Cauchy problem associated with the following stochastic scalar conservation laws

$$\begin{aligned} \frac{\partial u}{\partial t} + \frac{\partial}{\partial x} F(X, u) &= 0, & (x, t) \in \mathbb{R} \times (t_0, T], \\ u(t_0, x) &= u_0(x), & x \in \mathbb{R}, \end{aligned} \tag{1}$$

where $(t_0, T]$ is the time interval, $u \in \mathbb{R}$ is the scalar unknown, the flux function $F(X, u) : \Omega \times \mathbb{R} \longrightarrow \mathbb{R}$ is nonlinear, $u_0(x)$ is an initial condition given at time t_0 , and X is a stochastic process that can depend on space or/and time variable as well. In the deterministic case (with $X = k(x)$), the multiplicative flux function

$$F(k(x), u) = k(x)G(u), \quad k(x) = \begin{cases} k_L, & \text{if } x < 0, \\ k_R, & \text{if } x > 0, \end{cases} \tag{2}$$

has been widely used in the literature for theoretical and numerical analysis of conservation laws with discontinuous flux function. In (2), $G(u)$ is a continuous flux function in \mathbb{R} , k_L and k_R are positive constants with $k_L \neq k_R$. In all cases, we assume that the Jacobian $F'(k(x), u) = \partial F(k(x), u)/\partial u$ is diagonalizable with real eigenvalues. It should be noted that hyperbolic equations of conservation laws with discontinuous flux function of type (2) occur in many physical applications, for example in transport models in porous media [10], sedimentation phenomena [6], resonant models [21] and vehicular traffic flows [28,15]. Most practical applications of these problems cannot be solved analytically and hence require numerical methods. One of the main difficulties in the analysis of problem (1)-(2) is the correct definition of a solution. It is well known that after a finite time the problem (1)-(2) does not in general possess a continuous solution even if the initial data u_0 is sufficiently smooth. Hence a solution of (1)-(2) has to be understood in the weak sense. Moreover, among the difficulties that arose when approximating solutions of (1)-(2) are numerical instability, poor shock and rarefaction resolutions, and even spurious numerical solutions, see for instance [1,25,39] and references are therein.

Our objective in this paper is to develop an efficient numerical method for solving the stochastic scalar conservation laws (1) equipped with a discontinuous

flux function of the form

$$F(X, u) = \left(1 - H_X(x)\right) f(u) + H_X(x) g(u), \quad (3)$$

where f and g are continuous flux functions, and $H_X(x)$ is a Heaviside function defined as

$$H_X(x) = \begin{cases} 1, & \text{if } P(x < X) = 1, \\ 0, & \text{if } P(x > X) = 1. \end{cases} \quad (4)$$

Here, the stochastic process X can be seen as a random interface separating two media with different physical properties. The location of this interface may be moving within the spatial domain and time interval according to the probability P . Examples of recent applications in stochastic interface models can be found in [2] for growing interfaces in quenched media, in [24] for composite materials with stochastic interface defects, in [8] for dynamics of ion transfer across liquid-liquid interfaces, and in [48] for random elliptic interface problems. The common practice in stochastic interface models is to analyze the kinetics obtained from transition-state theory independently from stochastic molecular dynamic simulations. In general, the interface equations derived from the microscopic rules using regularization procedure predict accurately the roughness. The main contribution of the present work is to present an efficient finite volume method for solving conservation laws with discontinuous flux functions subject to the stochastic interface equation (4). Note that by setting $X = 0$ and changing the stochastic function $H_X(x)$ in (3) to the standard Heaviside function, one recover the classical equations for deterministic conservation laws with discontinuous flux functions

$$F(u) = \begin{cases} f(u), & \text{if } x < 0, \\ g(u), & \text{if } x > 0. \end{cases} \quad (5)$$

This class of problems has been widely studied in the literature, see for example [1,25,39]. The considered conservation laws involve stochastic effect, which increases the difficulty for solving them. This makes the development of numerical methods for stochastic conservation laws more attractive.

To close the system of equations (1) and (3) an equation describing the evolution of X is required. In the current work, the equations prescribing the evolution of the velocity fluctuation V and the displacement X are solutions of the following system of stochastic differential equation (SDE)

$$\begin{aligned} dV &= a(X, V) dt + b(t) dW, & V(t_0) &= V_0, \\ dX &= V dt + \epsilon dW, & X(t_0) &= X_0, \end{aligned} \quad (6)$$

where $a(X, V)$ is a given drift function, $b(t)$ is a given diffusion function, W is a Wiener process, X_0 and V_0 are known initial conditions at time t_0 , and

ϵ is a constant characterizing the rate of dissipation in the SDE. Note that in the system (6), the two terms in the right-hand side of each equation may represent the effects of the turbulent flow on the solution and they depend on the Lagrangian time scale and the velocity fluctuation standard deviation. In practice, the drift term $a(X, V)$ refers to fluctuations caused by the large scales, whereas the diffusion term $b(t)$ is related to short term fluctuations. The new model (6) presented in this paper to detect the interface in the conservation laws (1) is similar to the stochastic model for molecular motion in fluid dynamic equations. In these models, the kinetic fluid equations are solved through the stochastic motion of particles

$$\begin{aligned} \frac{dV_i}{dt} &= -\frac{1}{\tau} (V_i - U_i) + \sqrt{\frac{4e_s}{3\tau}} \frac{dW_i}{dt}, \\ \frac{dX_i}{dt} &= V_i, \end{aligned} \tag{7}$$

where X_i is the position of the i th particle, V_i is the molecular velocity of the particle, τ is the relaxation time, e_s is the sensible energy of the fluid and U_i is its mean velocity, compare [23] among others. Here, at the microscopic scale, the equations (7) represent statistical moments of the particle ensemble in the particle location X at time t . The mean velocity U is equivalent to the fluid velocity measured on the macroscopic fluid dynamic scale according to the ergodic theorem [12]. Note that the conservation law (1) and the interface equation (6) are not fully coupled such that once the SDE (6) is solved for the interface X , the flux function $F(X, u)$ is updated using (3) and then used in the numerical solution of the conservation laws (1). A possible fully coupled version of the model consists on solving the following system of stochastic differential equations

$$\begin{aligned} du &= -\left(\frac{\partial}{\partial x} F(X, u)\right) dt + \sigma(t, x) dW, & u(t_0) &= u_0, \\ dV &= a(X, V) dt + b(t) dW, & V(t_0) &= V_0, \\ dX &= V dt + \epsilon dW, & X(t_0) &= X_0, \end{aligned} \tag{8}$$

where σ is the amplitude of the random noise to be defined accordingly. However, the drawback of considering the coupled system (8) lies on the huge amount of computational cost needed for its time and space discretizations and also on the two-scale aspect of the problem. Remark that, in general applications, the time scale for the first equation in (8) is far different from the time scale in the two other equations. This may require an unacceptably small time steps to accurately capture the dynamics of the numerical solutions.

It should be stressed that the numerical techniques presented in this paper can be extended, without major conceptual modifications, to the generalized

stochastic conservation laws (1) with a flux function defined as

$$F\left(X^{(1)}, \dots, X^{(N)}, u\right) = H_{X^{(1)}} f_1(u) + \dots + H_{X^{(N)}} f_N(u), \quad (9)$$

where $f_k(u)$, with $k = 1, \dots, N$ are continuous flux functions, and $H_{X^{(k)}}(x)$ are Heaviside-type functions defined as

$$H_{X^{(k)}}(x) = \begin{cases} 1, & \text{if } P(x < X^{(k)}) = 1, \\ 0, & \text{if } P(x > X^{(k)}) = 1, \end{cases} \quad (10)$$

and satisfy the condition

$$H_{X^{(1)}}(x) + H_{X^{(2)}}(x) + \dots + H_{X^{(N)}}(x) = 1.$$

Note that $X^{(k)}$, with $k = 1, \dots, N$ can be seen as stochastic locations of the discontinuities in the flux function (9). As in the one-dimensional SDE (6), $\mathbf{V} = (V^{(1)}, \dots, V^{(N)})^T$ and $\mathbf{X} = (X^{(1)}, \dots, X^{(N)})^T$ represent respectively, the N -vector of velocity fluctuations and stochastic processes solving the following system of stochastic differential equations

$$\begin{aligned} d\mathbf{V} &= \mathcal{A}(\mathbf{X}, \mathbf{V}) dt + \mathcal{B}(t) d\mathbf{W}, & \mathbf{V}(t_0) &= \mathbf{V}_0, \\ d\mathbf{X} &= \mathbf{V} dt + \epsilon d\mathbf{W}, & \mathbf{X}(t_0) &= \mathbf{X}_0, \end{aligned} \quad (11)$$

where $\mathcal{A}(\mathbf{X}, \mathbf{V})$ is the drift N -vector, $\mathcal{B}(t)$ is the diffusion $N \times d$ -matrix, \mathbf{W} is a d -vector Wiener process, \mathbf{X}_0 and \mathbf{V}_0 are known N -vector of initial conditions given at time t_0 . Here, each entry of the d -vector \mathbf{W} forms a Brownian motion which is independent of the other elements.

It is worth pointing out that in general, it is difficult to derive an effective equation to be solved for the the average solution. However, for a fixed velocity the interface motion is governed by the SDE

$$dX = V dt + \epsilon dW, \quad (12)$$

where the position $X(t)$ process is Markovian and the evolution of its probability density function $p(t, x)$, is described by an advection-diffusion type of partial differential equation known as the Fokker-Planck equation [22]

$$\frac{\partial p}{\partial t} + \frac{\partial}{\partial x} (Vp) - \frac{1}{2} \frac{\partial^2}{\partial x^2} (\epsilon^2 p) = 0. \quad (13)$$

The initial spreading of a cloud of particles is very small and its distribution can be modelled using a Dirac delta function as

$$p(0, x) = \delta(x - x_0).$$

By assuming a zero diffusion and divergence-free velocity the equation (13) reduces to the advection equation for the interface ϕ

$$\frac{\partial \phi}{\partial t} + V \frac{\partial \phi}{\partial x} = 0, \quad (14)$$

that is similar to the interface equation widely used in level set methods (see for example [31]) in the sense that it replaces the microscopic model by a simpler model, namely Fokker-Planck model, but due to the implementation as particle method no discretization of the distribution function is necessary. Indeed, by interpreting the Fokker-Planck equation (13) as an advection equation makes the stochastic model in (6) to be consistent with the well-known interfacial flows used in the computational fluids dynamics.

3 Finite volume method for the stochastic conservation laws

Finite volume methods are preferable in numerical solutions of partial differential equations of hyperbolic type due to their conservation properties. These techniques have been developed mainly under assumptions of ideal input such as deterministic flux functions, initial data and computational domain. In practice, this is hardly the case as the flux functions and the input data involve uncertainties. In the current study, we propose a new finite volume method for stochastic conservation laws (1). To formulate our method, we discretize the spatial domain into control volumes $[x_{i-1/2}, x_{i+1/2}]$ with uniform size $\Delta x = x_{i+1/2} - x_{i-1/2}$ for simplicity. We also divide the time interval $[t_0, T]$ into subintervals $[t_n, t_{n+1}]$ with uniform size Δt . Following the standard finite volume formulation, we integrate the considered equation (1) with respect to time and space over the domain $[t_n, t_{n+1}] \times [x_{i-1/2}, x_{i+1/2}]$ to obtain the following discrete equation

$$U_i^{n+1} = U_i^n - \frac{\Delta t}{\Delta x} \left(F(X^{n+1}, U_{i+1/2}^n) - F(X^{n+1}, U_{i-1/2}^n) \right), \quad (15)$$

where X^{n+1} denotes an approximation of the stochastic process X at time t_{n+1} , $U_{i\pm 1/2}^n = u(t_n, x_{i\pm 1/2})$, U_i^n is the space average of the solution u in the domain $[x_{i-1/2}, x_{i+1/2}]$ at time t_n *i.e.*,

$$U_i^n = \frac{1}{\Delta t \Delta x} \int_{t_n}^{t_{n+1}} \int_{x_{i-1/2}}^{x_{i+1/2}} u(t, x) dt dx,$$

and $F(X^{n+1}, U_{i\pm 1/2}^n)$ is the numerical flux at $x = x_{i\pm 1/2}$ and time t_n . The spatial discretization of the equation (15) is complete when a numerical approximation of X^{n+1} is computed by solving the SDE (6) and a construction of the numerical fluxes $F(X^{n+1}, U_{i\pm 1/2}^n)$ is chosen. In what follows we discuss the formulation of a modified Rusanov method for the numerical approximation of the fluxes and we also formulate a stochastic Runge-Kutta scheme for the numerical solution of the system of stochastic differential equations.

3.1 A modified Rusanov method for spatial discretization

In general, the construction of the numerical fluxes $F(X^{n+1}, U_{i\pm 1/2}^n)$ in the finite volume discretization (15) requires a solution of Riemann problems at the cell interfaces $x_{i\pm 1/2}$. Let us assume that the self-similar solution to the Riemann problem associated with the equation (1) subject to the initial condition

$$u(0, x) = \begin{cases} U_L, & \text{if } x < 0, \\ U_R, & \text{if } x > 0, \end{cases} \quad (16)$$

is given by

$$u(t, x) = R_s \left(\frac{x}{t}, U_L, U_R \right),$$

where R_s is the Riemann solution which has to be either calculated exactly or approximated. Thus, the intermediate state $U_{i+1/2}^n$ in (15) at the cell interface $x = x_{i+1/2}$ is defined as

$$U_{i+1/2}^n = R_s \left(0, U_i^n, U_{i+1}^n \right). \quad (17)$$

From a computational viewpoint, this procedure is very demanding and may restricts the application of the method for which Riemann solutions are difficult to approximate or simply are not available. In order to avoid these numerical difficulties and reconstruct an approximation of $U_{i+1/2}^n$, we adapt a modified Rusanov method proposed in [30] for numerical solution of conservation laws. The central idea is to integrate the equation (1) over a control domain $[t_n, t_n + \theta_{i+1/2}^n] \times [x^-, x^+]$ containing the point $(t_n, x_{i+1/2})$ as depicted in Figure 1. Notice that, the integration of the equation (1) over the control domain $[t_n, t_n + \theta_{i+1/2}^n] \times [x^-, x^+]$ is used only at a predictor stage to construct the intermediate states $U_{i\pm 1/2}^n$ which will be used in the corrector stage (15). Here, $U_{i\pm 1/2}^n$ can be viewed as an approximation of the averaged Riemann solution R_s over the control volume $[x^-, x^+]$ at time $t_n + \theta_{i+1/2}^n$. Thus, the resulting intermediate state is given by

$$\int_{x^-}^{x^+} u(t_n + \theta_{i+1/2}^n, x) dx = \Delta x^- U_i^n + \Delta x^+ U_{i+1}^n - \theta_{i+1/2}^n \left(F(X^{n+1}, U_{i+1}^n) - F(X^{n+1}, U_i^n) \right), \quad (18)$$

where U_i^n denotes the space average of the solution u in the cell $[x^-, x^+]$ at time t_n given by

$$U_i^n = \frac{1}{\Delta x^- + \Delta x^+} \int_{x^-}^{x^+} u(t_n, x) dx, \quad (19)$$

and the distance measures Δx^- and Δx^+ are defined as

$$\Delta x^- = |x^- - x_{i+1/2}|, \quad \Delta x^+ = |x^+ - x_{i+1/2}|.$$

slopes $\alpha_{i+1/2}^n$ leading to a first-order scheme is $\alpha_{i+1/2}^n = \tilde{\alpha}_{i+1/2}^n$ with

$$\tilde{\alpha}_{i+1/2}^n = \frac{S_{i+1/2}^n}{s_{i+1/2}^n}, \quad (24)$$

where

$$s_{i+1/2}^n = \min\left(\left|F'(X^{n+1}, U_i^n)\right|, \left|F'(X^{n+1}, U_{i+1}^n)\right|\right).$$

In the present work, we consider a second-order scheme incorporating limiters in its reconstruction as

$$\alpha_{i+1/2}^n = \tilde{\alpha}_{i+1/2}^n + \sigma_{i+1/2}^n \Phi\left(r_{i+1/2}\right), \quad (25)$$

where $\tilde{\alpha}_{i+1/2}^n$ is given by (24) and $\Phi_{i+1/2} = \Phi\left(r_{i+1/2}\right)$ is an appropriate limiter which is defined by using a flux limiter function Φ acting on a quantity that measures the ratio $r_{i+1/2}$ of the upwind change to the local change, compare for instance [42]. Thus,

$$\sigma_{i+1/2}^n = \frac{\Delta t}{\Delta x} S_{i+1/2}^n - \frac{S_{i+1/2}^n}{s_{i+1/2}^n},$$

and the ratio of the upwind change is calculated locally as

$$r_{i+1/2} = \frac{U_{i+1-q} - U_{i-q}}{U_{i+1} - U_i}, \quad q = \text{sgn}\left[F'(X^{n+1}, U_{i+1/2}^n)\right].$$

As slope limiter functions, we consider the Minmod function

$$\Phi(r) = \max(0, \min(1, r)), \quad (26)$$

and the van Albada function

$$\Phi(r) = \frac{r + r^2}{1 + r^2}. \quad (27)$$

Note that other slope limiter functions such as van Leer or Superbee functions from [33,27] can also apply. The reconstructed slopes (25) are inserted into (22) and the numerical fluxes $U_{i+1/2}^n$ are computed from (20). Remark that if we set $\Phi = 0$, the spatial discretization (25) reduces to the first-order scheme.

3.2 Stochastic Runge-Kutta schemes for time integration

The modified Rusanov scheme proposed in the previous section is applied to the conservation laws (1) provided the location of the discontinuity X in the flux function is known a priori. For the deterministic flux function (2), this step does not require any further calculations. However, in the stochastic case,

a numerical solution of the SDE (6) is needed as a preprocessing step. Let us rewrite the system (6) in a vector form as

$$d\mathbf{Y} = \mathcal{F}(t, \mathbf{Y}) dt + \mathcal{G}(t) d\mathbf{W}, \quad \mathbf{Y}(t_0) = \mathbf{Y}_0, \quad (28)$$

where

$$\mathbf{Y} = \begin{pmatrix} V \\ X \end{pmatrix}, \quad \mathcal{F}(t, \mathbf{Y}) = \begin{pmatrix} a(X, V) \\ V \end{pmatrix}, \quad \mathcal{G}(t) = \begin{pmatrix} b(X, V) & 0 \\ 0 & \epsilon \end{pmatrix}.$$

Applied to the equation (28), the canonical Euler-Maruyama method yields

$$\begin{aligned} \mathbf{Y}^0 &= \mathbf{Y}_0, \\ \mathbf{Y}^{n+1} &= \mathbf{Y}^n + \mathcal{F}(t_n, \mathbf{Y}^n) \Delta t + \mathcal{G}(t_n) \Delta \mathbf{W}, \quad n = 0, 1, \dots, \end{aligned} \quad (29)$$

where \mathbf{Y}^n is the approximation of the stochastic process \mathbf{Y}_t at a time $t = t_n$ and $\Delta \mathbf{W}$ is the Brownian increment $\mathcal{N}(0, \sqrt{\Delta t})$. It is well-known that the Euler-Maruyama scheme (29) is only $\mathcal{O}((\Delta t)^{0.5})$ accurate, see for example [26]. As described in the previous section, the spatial discretization is $\mathcal{O}((\Delta x)^2)$ accurate. Therefore, in order to preserve an overall second-order accuracy in the presented method, it is necessary that the time integration of the SDE (28) should be at least $\mathcal{O}((\Delta t)^2)$ accurate.

In the present work, we apply a class of stochastic Runge-Kutta (SRK) methods studied in [35–37] for the numerical solution of systems of stochastic differential equations. The methods exhibit a weak convergence with second order in the case of additive noise. Thus, the considered error of the SRK approximation \mathbf{Y} is bounded as

$$\left| \langle \psi(\mathbf{Y}^n) \rangle - \langle \psi(\mathbf{Y}(t_n)) \rangle \right| \leq C_\psi (\Delta t)^2,$$

with some constant $C_\psi > 0$ for all functionals $\psi \in C_p^6(\mathbb{R}^2, \mathbb{R})$ with polynomial growth and sufficient small time step Δt , see for example [36]. The s -stage SRK method applied to the SDE (28) is given by

$$\begin{aligned} \mathbf{Y}^0 &= \mathbf{Y}_0, \\ \mathbf{Y}^{n+1} &= \mathbf{Y}^n + \sum_{i=1}^s \alpha_i \mathcal{F}(t_n + c_i \Delta t, \mathbf{H}_i) \Delta t + \sum_{k=1}^2 \sum_{i=1}^s \beta_{ik} \mathcal{G}^{(k)}(t_n) \hat{I}^{(k)}, \end{aligned} \quad (30)$$

where the SRK stages \mathbf{H}_i , with $i = 1, \dots, s$ are defined as

$$\mathbf{H}_i = \mathbf{Y}^n + \sum_{j=1}^s A_{ij} \mathcal{F}(t_n + c_j \Delta t, \mathbf{H}_j) \Delta t + \sum_{l=1}^2 \sum_{j=1}^s B_{ij} \mathcal{G}^{(l)}(t_n) \hat{I}^{(l)}. \quad (31)$$

According to the definition of the diffusion matrix in (28), $\mathcal{G}^{(1)}(t) = b(t)$ and $\mathcal{G}^{(2)}(t) = \epsilon$. The random variables $\hat{I}^{(k)}$ used by the SRK method are, for example, independent identically $\mathcal{N}(0, \Delta t)$ distributed or simply independent identically distributed with

$$\mathrm{P}\left(\hat{I}^{(k)} = \pm\sqrt{3\Delta t}\right) = \frac{1}{6} \quad \text{and} \quad \mathrm{P}\left(\hat{I}^{(k)} = 0\right) = \frac{2}{3}, \quad k = 1, 2.$$

The coefficients α_i , c_i , β_i , A_{ij} and B_{ij} appeared in the SRK method (30)-(31) are usually given by the following extended Butcher tableau

$$\begin{array}{c|ccc|ccc} c_1 & A_{11} & \dots & A_{1s} & B_{11} & \dots & B_{1s} \\ \vdots & \vdots & \ddots & \vdots & \vdots & \ddots & \vdots \\ c_s & A_{s1} & \dots & A_{ss} & B_{s1} & \dots & B_{ss} \\ \hline & \alpha_1 & \dots & \alpha_s & \beta_1 & \dots & \beta_s \end{array}$$

Note that the considered SRK method (30) is a simplified version of the more general second-order SRK methods introduced in [37]. Since only additive noise is considered, many order conditions turn out to be automatically fulfilled. In the simulations presented in the present work, we have implemented an explicit SRK method with the number of stages $s = 2$. Its associated extended Butcher tableau is given by

$$\begin{array}{c|cc|cc} 0 & 0 & 0 & 0 & 0 \\ 1 & 1 & 0 & 1 & 0 \\ \hline & \frac{1}{2} & \frac{1}{2} & 1 & 0 \end{array} \quad (32)$$

In summary, the implementation of the proposed algorithm to solve the stochastic conservation law (1) is carried out in the following two steps. Given (X^n, U^n) , we compute (X^{n+1}, U^{n+1}) via:

Step 1. Solve for (X^{n+1}, V^{n+1}) the SDE (6) using the second-order SRK scheme as:

$$\begin{aligned} \mathbf{H}^n &= \mathbf{Y}^n + \mathcal{F}(t_n, \mathbf{Y}^n) \Delta t + \sum_{l=1}^2 \mathcal{G}^{(l)}(t_n) \hat{I}^{(l)}, \\ \mathbf{Y}^{n+1} &= \mathbf{Y}^n + \frac{1}{2} \mathcal{F}(t_n, \mathbf{Y}^n) \Delta t + \frac{1}{2} \mathcal{F}(t_n + \Delta t, \mathbf{H}^n) \Delta t + \sum_{l=1}^2 \mathcal{G}^{(l)}(t_n) \hat{I}^{(l)}, \end{aligned} \quad (33)$$

where \mathbf{Y} , \mathcal{F} and \mathcal{G} are defined in (28).

Step 2. Solve for U_i^{n+1} the conservation law (1) using the proposed predictor-corrector method as:

$$\begin{aligned}
U_{i+1/2}^n &= \frac{1}{2} (U_i^n + U_{i+1}^n) - \frac{\alpha_{i+1/2}^n}{2S_{i+1/2}^n} (F(X^{n+1}, U_{i+1}^n) - F(X^{n+1}, U_i^n)), \\
U_i^{n+1} &= U_i^n - \frac{\Delta t}{\Delta x} (F(X^{n+1}, U_{i+1/2}^n) - F(X^{n+1}, U_{i-1/2}^n)),
\end{aligned} \tag{34}$$

where $S_{i+1/2}^n$ and $\alpha_{i+1/2}^n$ are defined in (23) and (25), respectively.

It is evident that, due to the stochasticity in the conservation law (1), the above algorithm is used to generate a number M of realizations. Thus, a Monte Carlo simulation is performed for the solution samples U_m^n for $m = 1, \dots, M$, and we estimate the expectation of the solution U^{n+1} at time t_{n+1} by

$$\langle \psi(U^{n+1}) \rangle \approx \frac{1}{M} \sum_{m=1}^M \psi(U_m^{n+1}).$$

Note that other SRK methods from [37] can also be applied for solving the SDE system (28).

4 Numerical results

We present numerical results for several test problems to check the accuracy and the performance of the proposed finite volume method. As with all explicit time stepping methods the theoretical maximum stable time step Δt is specified according to the CFL condition

$$\Delta t = Cr \frac{\Delta x}{\max_i (|\alpha_{i+1/2}^n S_{i+1/2}^n|)}, \tag{35}$$

where Cr is a constant to be chosen less than unity. In all our simulations, the fixed Courant number $Cr = 0.75$ is used and the time step is varied according to (35). In all the simulations (unless stated) we perform $M = 1000$ realizations and mean solutions are displayed. The following test examples are selected:

4.1 Accuracy test problems

Our first example is a deterministic conservation law with exact steady-state solution which can be used to quantify the results obtained by the classical Rusanov method and the proposed modified Rusanov method. This example can also serve to test the ability of the above finite volume method to converge to the correct entropy solution. The problem statement is given by the

equations (1)-(2) where

$$G(u) = u(1 - u), \quad k(x) = \begin{cases} 2, & \text{if } 0 \leq x \leq 2.5, \\ \frac{25-2x}{10}, & \text{if } 2.5 < x < 7.5, \\ 1, & \text{if } 7.5 \leq x \leq 10, \end{cases} \quad (36)$$

and an initial condition given by

$$u_0(x) = \begin{cases} 0.9, & \text{if } 0 \leq x \leq 2.5, \\ \frac{1+\sqrt{0.28}}{2}, & \text{if } 2.5 < x \leq 10. \end{cases}$$

This problem has a steady exact solution given by

$$u_\infty(x) = \begin{cases} 0.9, & \text{if } 0 \leq x \leq 2.5, \\ \frac{1}{2} + \frac{\sqrt{k(x)^2 - 0.72k(x)}}{2k(x)}, & \text{if } 2.5 < x < 7.5, \\ \frac{1+\sqrt{0.28}}{2}, & \text{if } 7.5 \leq x \leq 10. \end{cases}$$

We compute the approximate solution at time $t = 20$. At this time the approximated solutions are almost stationary, and therefore error norms can be calculated. We consider the L^∞ -, L^1 - and L^2 -error norms defined as

$$\max_{1 \leq i \leq N} |U_i - u_\infty(x_i)|, \quad \sum_{i=1}^N |U_i - u_\infty(x_i)| \Delta x, \quad \sqrt{\sum_{i=1}^N |U_i - u_\infty(x_i)|^2 \Delta x},$$

respectively. Here, U_i and $u_\infty(x_i)$ are respectively, the computed and exact steady-state solutions at gridpoint x_i , whereas N stands for the number of gridpoints used in the spatial discretization. The obtained results for the classical Rusanov method are listed in Table 1 along with their corresponding convergence rates. Those corresponding to the proposed modified Rusanov method using the van Albada limiter are presented in Table 2. It reveals that increasing the number of gridpoints in the computational domain results in a decay of all considered error norms in both methods. The results provided by the modified Rusanov method are more accurate than the results provided by the classical Rusanov method. Our modified Rusanov method exhibits good convergence behavior for this nonlinear problem. As can be seen from the convergence rates presented in these tables, the classical Rusanov method shows only a first-order accuracy, whereas a second-order accuracy is achieved in our method for this test example in terms of the considered error norms. A similar trend has been observed in the errors (not reported here) obtained using the MinMod limiter in the proposed modified Rusanov method.

Next we examine the accuracy of the considered SRK scheme for solving stochastic differential equations. To this end we solve the linear stochastic

Table 1

Errors for the accuracy test problem (36) using the classical Rusanov method.

M	L^∞ -error	Rate	L^1 -error	Rate	L^2 -error	Rate
50	6.22252E-03	—	1.42606E-02	—	7.13845E-03	—
100	3.36303E-03	0.887	6.94884E-03	1.037	3.50372E-03	1.026
200	1.69172E-03	0.991	3.42991E-03	1.018	1.73552E-03	1.013
400	8.48215E-04	0.995	1.70387E-03	1.009	8.63612E-04	1.006
800	4.24668E-04	0.998	8.49169E-04	1.004	4.30760E-04	1.003

Table 2

Errors for the accuracy test problem (36) the modified Rusanov method.

M	L^∞ -error	Rate	L^1 -error	Rate	L^2 -error	Rate
50	1.84252E-04	—	2.98443E-04	—	1.68312E-04	—
100	5.35180E-05	1.783	7.23079E-05	2.045	4.27158E-05	1.978
200	1.36748E-05	1.968	1.79117E-05	2.013	1.06081E-05	2.009
400	3.45575E-06	1.984	4.45720E-06	2.006	2.64244E-06	2.005
800	8.68570E-07	1.992	1.11168E-06	2.003	6.59364E-07	2.002

differential equation

$$dX = \lambda(\mu - X)dt + \epsilon dW, \quad X(0) = X_0. \quad (37)$$

It is easy to verify that the expected analytical solution of (37) is given by

$$\bar{X}(t) = X_0 e^{-\lambda t} + \mu (1 - e^{-\lambda t}). \quad (38)$$

The exact solution (38) is also used to evaluate the expected error function at time t_n as

$$\mathcal{E}(t_n) = \left| \bar{X}(t_n) - \langle X^n \rangle \right|,$$

where $\bar{X}(t_n)$ and $\langle X^n \rangle$ are the expected exact and numerical solutions at time t_n , respectively. In our computations we use $\lambda = 1$, $\mu = 1.2$, $X_0 = 1$ and simulations are stopped at time $t_n = 2$. In Figure 2 we display the evolution in time of the error $\mathcal{E}(t)$ for the Euler-Maruyama and the SRK schemes using a uniform step size $\Delta t = 2^{-5}$ and two values of ϵ namely, $\epsilon = 0.01$ and $\epsilon = 0.3$. As expected, the errors in the SRK solutions are far too small compared to those in the Euler-Maruyama scheme. Larger errors are detected for larger values for ϵ in both schemes. It is evident that the stochastic fluctuations are more pronounced in the error plots for the simulation with $\epsilon = 0.3$ than for the case with $\epsilon = 0.01$. For this test example, we have used $M = 10000$ and it may be noted that this number of realizations were sufficient for a weak convergence of the computations. To illustrate this convergence behavior, we summarize in Table 3 the L^∞ -norm of the error $\mathcal{E}(t)$ using different time steps. Convergence rates for the Euler-Maruyama and SRK schemes are also reported in this table for the considered values of ϵ . A simple inspection of Table 3 reveals that a

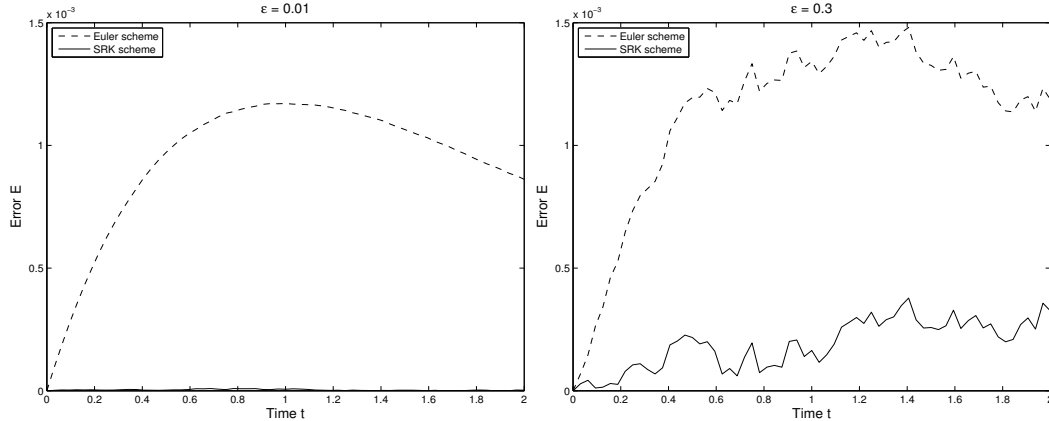


Fig. 2. Evolution of the error $\mathcal{E}(t)$ in the Euler-Maruyama and the SRK schemes for the linear SDE (37) using $\Delta t = 2^{-5}$. $\epsilon = 0.01$ (left plot) and $\epsilon = 0.3$ (right plot).

Table 3

Errors for the linear SDE (37) using the Euler-Maruyama and SRK schemes.

Δt	Euler scheme				SRK scheme			
	$\epsilon = 0.01$	Rate	$\epsilon = 0.3$	Rate	$\epsilon = 0.01$	Rate	$\epsilon = 0.3$	Rate
2^{-1}	$4.905E-03$	—	$5.156E-03$	—	$2.659E-03$	—	$8.832E-02$	—
2^{-2}	$3.566E-03$	0.46	$3.990E-03$	0.37	$6.788E-04$	1.97	$2.383E-02$	1.89
2^{-3}	$2.557E-03$	0.48	$2.962E-03$	0.43	$1.697E-04$	2.00	$6.125E-03$	1.96
2^{-4}	$1.796E-03$	0.51	$2.139E-03$	0.47	$3.986E-05$	2.09	$1.542E-03$	1.99
2^{-5}	$1.210E-03$	0.57	$1.513E-03$	0.50	$9.108E-06$	2.13	$3.778E-04$	2.03

decay of the error norm is achieved by decreasing the time steps for both schemes. However, a faster decay has been observed in the error computed using the SRK scheme. As can be seen, the rate of convergence in the Euler-Maruyama scheme is of $\mathcal{O}((\Delta t)^{0.5})$ whereas the SRK scheme exhibits a second-order accuracy for the considered values of ϵ . It should be stressed that, in our simulations the computational time required for the SRK scheme is about 2.3 times the computational time needed for the Euler-Maruyama scheme.

4.2 Stochastic Burgers flow problem

We first consider the deterministic inviscid Burgers equation with discontinuous flux function given by (2) with

$$G(u) = \frac{1}{2}u^2, \quad k(x) = \begin{cases} 1, & \text{if } x < 5, \\ 3, & \text{if } x > 5, \end{cases} \quad (39)$$

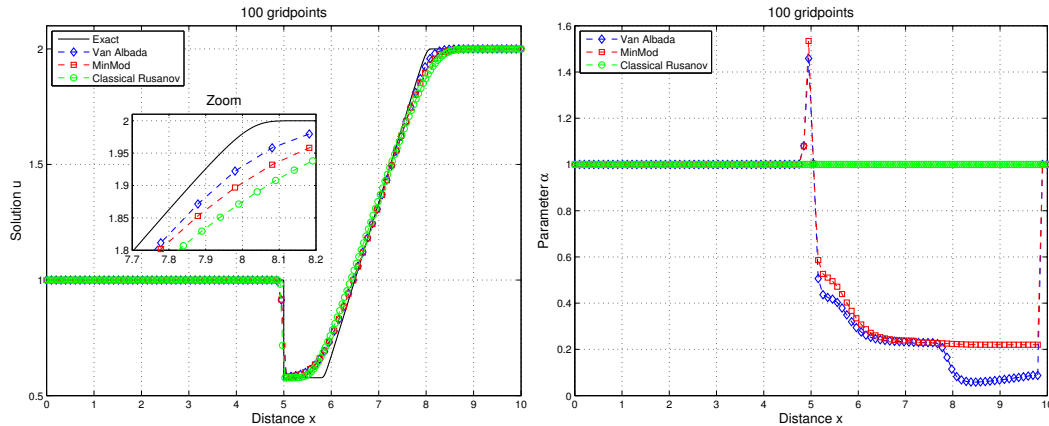


Fig. 3. Comparison of different limiters for the deterministic Burgers equation (left plot) and their corresponding parameter $\alpha_{i+1/2}$ (right plot) at time $t = 0.5$.

and an initial condition given by

$$u_0(x) = \begin{cases} 1, & \text{if } x < 5, \\ 2, & \text{if } x > 5. \end{cases} \quad (40)$$

In a first run with this test example, we compare the results obtained using the two considered limiter functions (26) and (27) in the modified Rusanov method on a mesh with 100 gridpoints. In the left plot in Figure 3 we display the computed solutions at time $t = 0.5$ along with a reference solution obtained by applying the method on the very fine mesh of 10000 gridpoints. For comparison reasons, we have also included the solution computed with the classical Rusanov method. Note that for a better comparison, a zoom of the solutions is included within the results. It is clear from the results presented in this figure that the numerical diffusion is more pronounced in the results obtained using the classical Rusanov scheme. This excessive numerical dissipation has been successfully removed by using the modified Rusanov method with both the MinMod and the van Albada limiters. It is seen that for the considered conditions, the van Albada limiter gives better results followed by the MinMod limiter. The associated selection of the parameter $\alpha_{i+1/2}$ in these methods is depicted in the right plot in Figure 3. As mentioned earlier in the classical Rusanov method, $\alpha_{i+1/2} = 1$ and it remains constant while a locally variable $\alpha_{i+1/2}$ is used in the proposed modified Rusanov method. This variation in $\alpha_{i+1/2}$ has been detected in the area on the computational domain where the shock and rarefaction waves appear. Different features are observed in the plots of $\alpha_{i+1/2}$ using the MinMod and the van Albada limiters. Hence, our next computations with the modified Rusanov method will be realized with the van Albada limiter only.

Next we compare the performance of the proposed finite volume method to the well-established Roe method [34]. The computed results using a mesh with 100 and 200 gridpoints are depicted in Figure 4. It is seen that for this

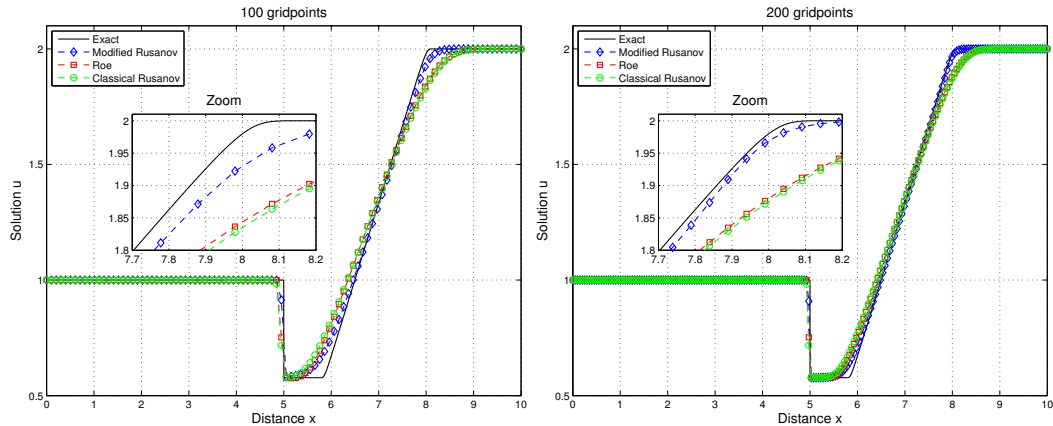


Fig. 4. Comparison of different methods for the deterministic Burgers equation using 100 gridpoints (left plot) and 200 gridpoints (right plot) at time $t = 0.5$.

test example, the results obtained using the classical Rusanov and the Roe methods are roughly the same. For both meshes, the proposed finite volume method is more accurate, as it is clearly seen in the vicinity of the shock and the contact waves. The modified Rusanov method offers a fine approximation to the solution since it removes the smearing of the classical Rusanov and Roe methods produced in the shock. For the considered meshes, it has been found that the proposed finite volume method requires three to four times less computational work than the Roe scheme. We have also found that the CPU time needed for the modified Rusanov method is less than 1.5 times more than that needed for the classical method. The additional computational effort used by the procedure in the selection of the parameter $\alpha_{i+1/2}$ has been kept to the minimum that the modified method is still effective. The proposed finite volume method seems to be a good compromise between the accuracy and the computational efficiency.

Our next concern is to examine the performance of the proposed finite volume method for solving stochastic Burgers equations. Therefore, we solve the stochastic conservation law (1) subject to the following flux function

$$F(\mathcal{K}(x), u) = \mathcal{K}(x) \frac{u^2}{2}, \quad \mathcal{K}(x) = \begin{cases} 1, & \text{if } x < X, \\ 3, & \text{if } x > X, \end{cases} \quad (41)$$

and the initial condition (40). The governing stochastic differential equations for the velocity fluctuation V and the displacement X are

$$\begin{aligned} dV &= 0.4 \cos(\pi X) dt + 0.5e^{-0.5t^2} dW, & V(0) &= 0, \\ dX &= V dt + \epsilon dW, & X(0) &= 5. \end{aligned} \quad (42)$$

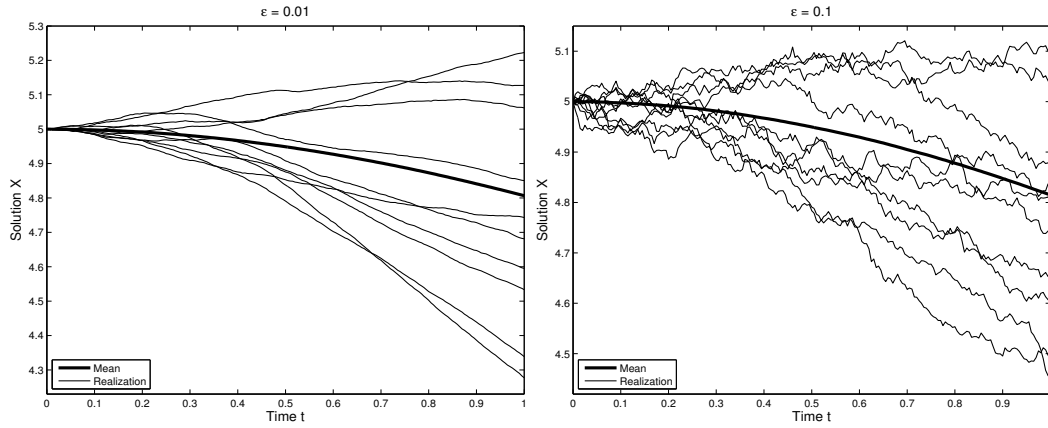


Fig. 5. Sample paths for the trajectory X along with the mean value of X in the stochastic Burgers equation with $\epsilon = 0.01$ (left plot) and $\epsilon = 0.1$ (right plot).

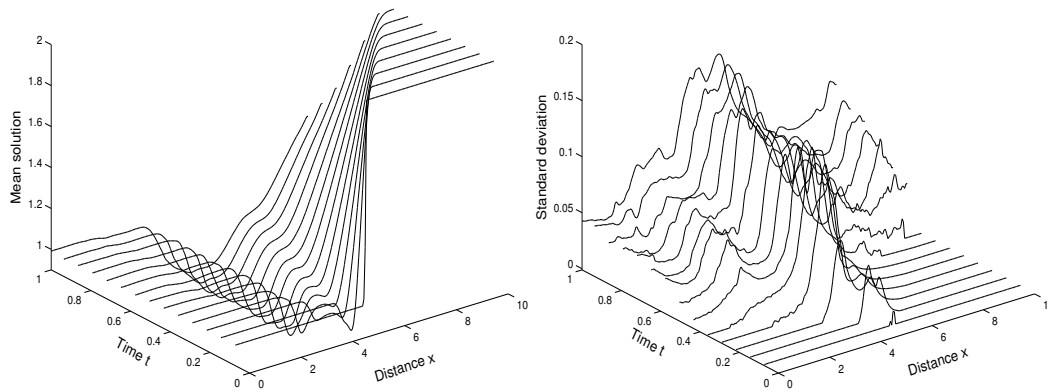


Fig. 6. Evolution in the time-space domain of the expected solution (left plot) and the standard deviation (right plot) for the stochastic Burgers equation with $\epsilon = 0.01$.

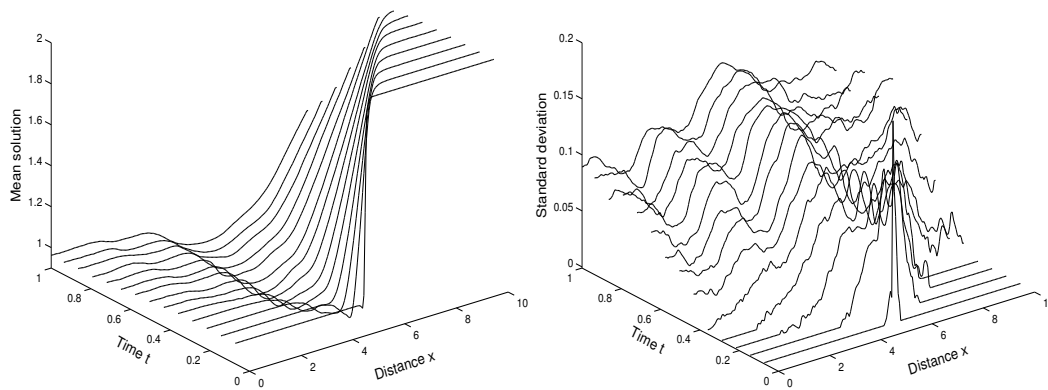


Fig. 7. Evolution in the time-space domain of the expected solution (left plot) and the standard deviation (right plot) for the stochastic Burgers equation with $\epsilon = 0.1$.

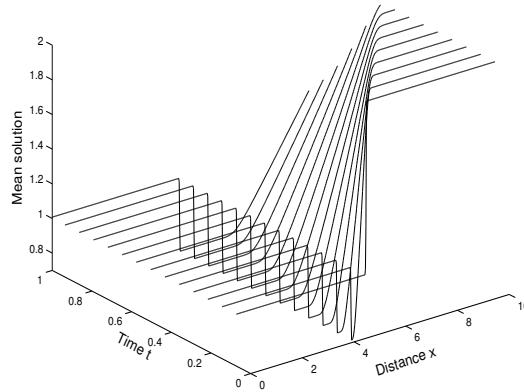


Fig. 8. Evolution in the time-space phase domain of the numerical solution for the deterministic Burgers equation.

In Figure 5 we show 10 independent sample paths along with the mean solution of the displacement X computed using the SRK scheme with $\epsilon = 0.01$ and $\epsilon = 0.1$. A large perturbation is obtained for large values of ϵ and the noise in the trajectories become more clear for larger values of ϵ . As can be seen, in this test example, the expected interface is no longer the constant $X = 5$ as in the deterministic flux (39). It is therefore, evident that the stochastic solution exhibits different behavior than that illustrated for the deterministic solution. The SRK scheme performs well for solving the nonlinear system of stochastic differential equations (42).

The evolution in time-space phase domain of the mean solutions and their corresponding standard variations is presented in Figure 6 and Figure 7 for $\epsilon = 0.01$ and for $\epsilon = 0.1$, respectively. For these results we have used a mesh with 200 gridpoints to reduce the grid dependence in the simulated results. As can be seen from these figures, smaller standard deviations are obtained for smaller values of stochastic magnitudes ϵ . It also seen that the variation of the variance solutions is large and the maximum values are located along the shock line. The proposed finite volume method accurately resolves this stochastic conservation law without exhibiting nonphysical oscillations. It is clear that the uncertainty in the considered Burgers equation seems to play a diffusion role in the problem, compare the resolution of shocks in the results presented in Figure 6 and Figure 7. For the sake of comparison, we illustrate in Figure 8 the evolution in the time-space domain of the numerical solution of the deterministic Burgers equation (40). Notice that increasing the value of ϵ , the numerical expected solutions in the stochastic simulations deviate from the solutions in the deterministic situation. The performance of the modified Rusanov method and the stochastic Runge-Kutta scheme is very attractive since the computed solutions remain stable and accurate even for relatively coarse meshes without solving Riemann problems or requiring complicated representation of the uncertainty.

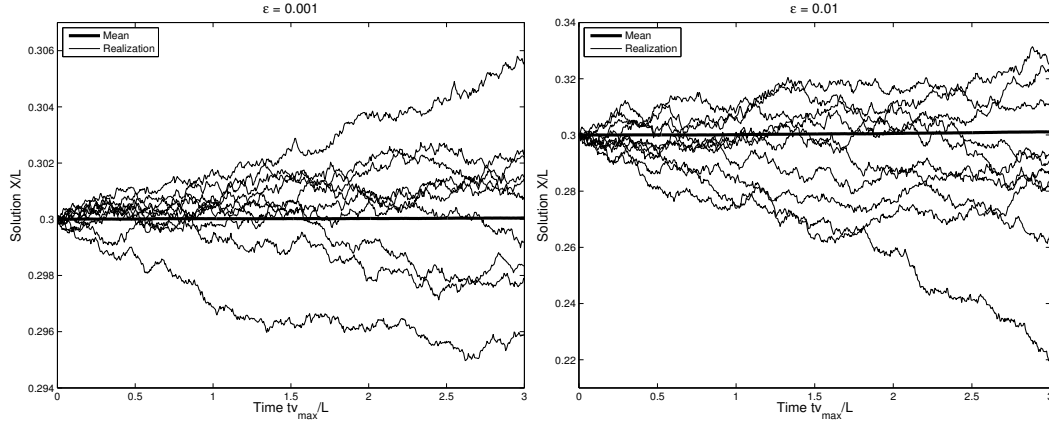


Fig. 9. Sample paths for the trajectory X along with the mean value of X in the stochastic traffic flow problem with $\epsilon = 0.001$ (left plot) and $\epsilon = 0.01$ (right plot).

4.3 Stochastic traffic flow problem

Traffic flow models remain challenging for numerical solution, even though great progress has been made in the development of modern shock capturing methods for equations of conservation laws in the last decades. Taking into account the nature of vehicular roads and the behavior of drivers, these models offer a realistic one-dimensional conservation law with stochastic discontinuous coefficient entries, see for example [41]. The well-known Lighthill-Whitham and Richards model [28] for traffic flows can be formulated in a conservation law of the form (1) where

$$u(t, x) = a(x)\rho(t, x),$$

with $a(x)$ and $\rho(t, x)$ are the lane number and the density per-lane, respectively. In this example, we consider a stochastic flux function given by

$$F(\mathcal{K}(x), u) = \mathcal{K}(x)u(1 - u), \quad \mathcal{K}(x) = \frac{v(t, x)}{v_{max}}, \quad (43)$$

where $v(t, x)$ is the free flow velocity at the location x and v_{max} is the maximum allowable speed. Here, we consider a road with length of $L = 10$ Km with an initial density $\rho(x) = 0.2$ veh/Km. The coefficients $a(x)$ and $v(t, x)$ are stochastic discontinuous functions given by

$$a(x) = \begin{cases} 4, & \text{if } x < X, \\ 2, & \text{if } x \geq X, \end{cases} \quad v(t, x) = \begin{cases} 1, & \text{if } x < X, \\ 0.6, & \text{if } x \geq X. \end{cases} \quad (44)$$

In this example, the SDE we used to model the velocity fluctuation V and the displacement X are given as

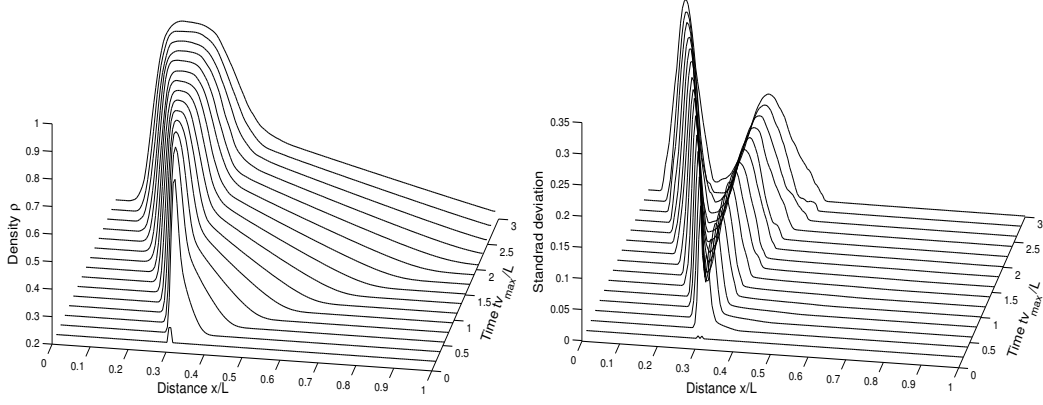


Fig. 10. Evolution in the time-space domain of the expected solution (left plot) and the standard deviation (right plot) for the stochastic traffic problem with $\epsilon = 0.001$.

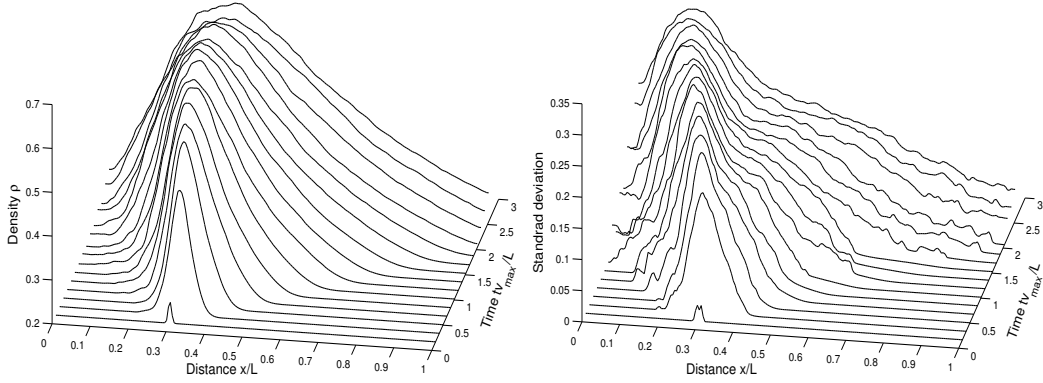


Fig. 11. Evolution in the time-space domain of the expected solution (left plot) and the standard deviation (right plot) for the stochastic traffic problem with $\epsilon = 0.01$.

$$\begin{aligned} \frac{1}{\epsilon}dV &= \left(\frac{1}{2} - V\right) X^3 dt + dW, & V(0) &= 0 \text{ Km/h}, \\ dX &= V dt + \epsilon dW, & X(0) &= 3 \text{ Km}. \end{aligned} \tag{45}$$

The computational road is divided into 200 gridpoints and the duration of this simulation is 900 s. To display the results we use dimensionless variables obtained by scaling the space x and time t by x/L and tv_{max}/L , respectively.

Figure 9 shows 10 independent sample paths along with the mean solution of the dimensionless displacement X obtained by solving the SDE (45) using the SRK scheme with $\epsilon = 0.001$ and $\epsilon = 0.01$. This Figure reveals that the magnitude of the noise in the stochastic traffic flow problem increases as the values of ϵ become large. Note that, unlike the previous test example, for the considered test problem, the expected value of the trajectory X remains constant and equals to 3 Km for both values of ϵ . The SRK scheme captures the correct dynamics of the displacement in the nonlinear system of stochastic

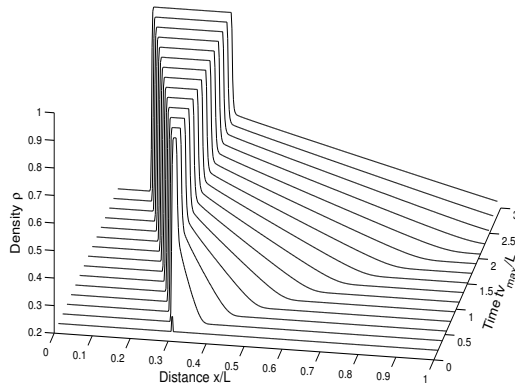


Fig. 12. Evolution in the time-space phase domain of the numerical solution for the deterministic traffic flow problem.

differential equations (45). It is worth mentioning that a deterioration of the accuracy in solving the system (45) will consequently result in a degradation of the accuracy in the finite volume solution of the traffic flow problem (43).

In Figure 10 and Figure 11 we present the evolution in time-space phase domain of the dimensionless mean density solutions and their corresponding standard variations for $\epsilon = 0.001$ and for $\epsilon = 0.01$, respectively. Note that for a larger diffusion coefficient ϵ , the effects of uncertainties are more pronounced in the expected solutions. This can be attributed to the fact that a stochastic flux function adds numerical diffusion to the traffic flow problem which could be neglected if a physical diffusion is introduced in the original problem. We observe that the standard deviation attains the highest values in the regions of a steep gradient. Apparently, the overall traffic flow features for this example are preserved with no spurious oscillations appearing in the results obtained using the proposed methods. Obviously, the computed results verify the stability and the shock capturing properties of the proposed finite volume method.

The evolution of the deterministic dimensionless density (obtained using fixed $X = 3 \text{ Km}$ in (44)) is shown in Figure 12. Our finite volume method captures the correct traffic jam structure and it advects the moving fronts without deteriorating the location of backwards and forwards waves. It is also clear that by using a limiting procedure in the local selection of the parameter $\alpha_{i+1/2}$ in (25), high resolution is obtained in those regions where the gradients of the solution are steep such as the moving fronts. Remark that although the expected trajectory in the SDE (45) is $X = 3 \text{ Km}$, the obtained stochastic and deterministic solutions are not similar. For example, the shock is better captured in the deterministic solution than its stochastic counterpart, and diffusion is more pronounced in the stochastic solution than the deterministic one. Our method accurately resolves this nonlinear stochastic traffic flow problem.

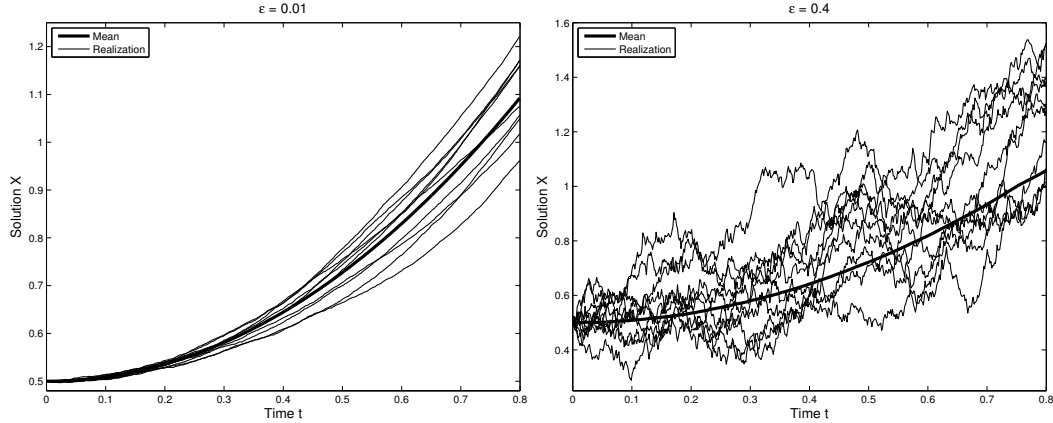


Fig. 13. Sample paths for X along with the mean solution for the stochastic Buckley-Leverett problem with $\epsilon = 0.01$ (left plot) and $\epsilon = 0.4$ (right plot).

4.4 Stochastic two-phase flow problem

The Buckley-Leverett equation has served as one of the simplest model of two-phase flow in a stochastic porous medium, see for example [18]. Here the governing equations are (1) where the flux function is not convex and it is given by

$$F(\mathcal{K}(x), u) = \frac{u^2}{u^2 + \mathcal{K}(x)(1-u)^2}, \quad \mathcal{K}(x) = \begin{cases} 50, & \text{if } x < X, \\ 5, & \text{if } x > X. \end{cases} \quad (46)$$

The initial condition is

$$u_0(x) = \begin{cases} 0, & \text{if } 0 \leq x \leq 1 - \frac{1}{\sqrt{2}}, \\ 1, & \text{if } 1 - \frac{1}{\sqrt{2}} \leq x \leq 1. \end{cases}$$

In this example, the SDE we used to model the velocity fluctuation V and the displacement X are given as

$$\begin{aligned} dV &= \frac{2Xu(1-u)}{((1+X)u^2 - 2Xu + X)^2} dt + \frac{t}{1+t} dW, & V(0) &= 0, \\ dX &= V dt + \epsilon dW, & X(0) &= 0.5. \end{aligned} \quad (47)$$

This problem is more complicated than the previous one since the drift term in the first equation in (47) depends on the displacement X and the solution u as well. Recall that this drift term is obtained by differentiating the flux function $F(X, u)$ with respect to u . In order to illustrate the stochastic nature of the solutions in the system (47), we generate the trajectories for the solution u computed at the point $x = 0.5$. In Figure 13 we present 10 independent sample paths along with the mean solution of the displacement X computed using the

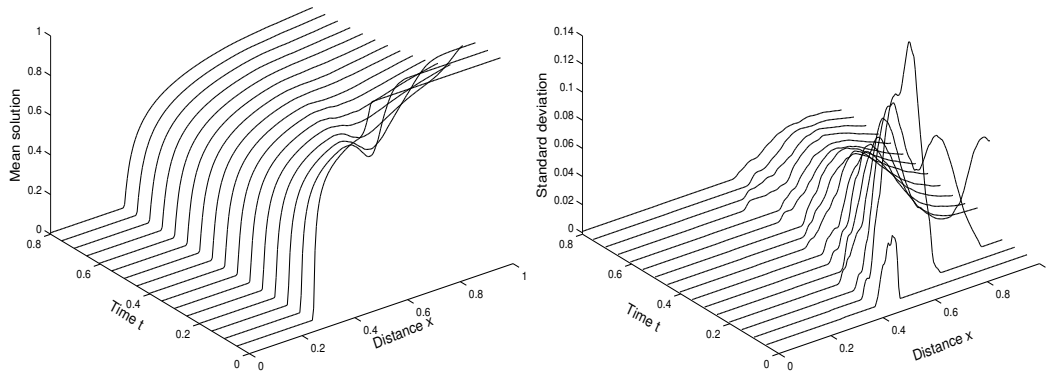


Fig. 14. Evolution in the time-space phase domain of the expected solution (left plot) and the standard deviation (right plot) for the stochastic Buckley-Leverett problem with $\epsilon = 0.01$.

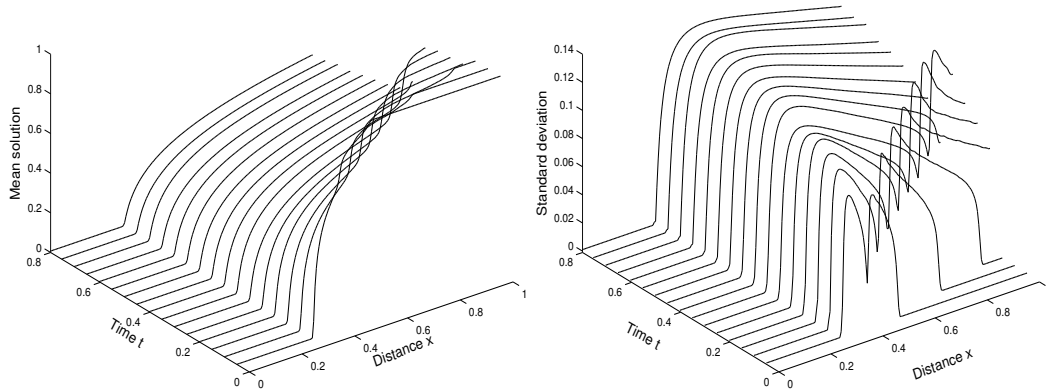


Fig. 15. Evolution in the time-space phase domain of the expected solution (left plot) and the standard deviation (right plot) for the stochastic Buckley-Leverett problem with $\epsilon = 0.4$.

SRK scheme with $\epsilon = 0.01$ and $\epsilon = 0.4$. Larger fluctuations are detected in the trajectories obtained for $\epsilon = 0.4$. As can be seen, good behavior is recovered by the SRK scheme for the considered stochastic inputs in the system (47) without any significant loss of accuracy.

The evolution in time-space phase domain of the mean solutions and their corresponding standard variations is presented in Figure 14 and Figure 15 for $\epsilon = 0.01$ and for $\epsilon = 0.4$, respectively. For sake of completion, we also present in Figure 16 the evolution in the time-space domain of the solution of the deterministic Buckley-Leverett problem obtained by setting $X = 0.5$ in (46). In all these results, the spatial domain is discretized into 200 gridpoints. Note that the exact solutions to these examples are not available, but the computed solutions using the proposed method seem to converge to the physically relevant solutions in all selected test cases. The proposed finite volume method captures the shock accurately, does not diffuse the fronts or gives oscillations

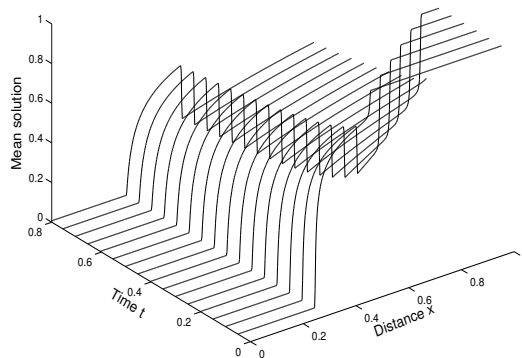


Fig. 16. Evolution in the time-space phase domain of the numerical solution for the deterministic Buckley-Leverett problem.

near the steep gradients. As can be seen, larger deformation and diffusion have been detected in the stochastic solutions than those obtained for the deterministic problem. For the considered random perturbations in the SDE (47), the stochastic location of the interface in the flux function acts like diffusion in the sense that the computed solutions are damped. Note that, the random external force in the stochastic differential equations (47) does not directly contribute to the mean solution of the Buckley-Leverett problem. However, due to the nonlinearity of the equations, the mean solution is driven by the velocity fluctuation V and the displacement X that represent the uncertainty of the solution.

5 Conclusions

A simple and accurate finite volume Runge-Kutta method to solve the scalar conservation laws with stochastic time-space dependent flux function has been presented. The method combines the attractive attributes of the finite volume method for spatial discretization and the stochastic Runge-Kutta scheme for time integration to yield a procedure for either linear or nonlinear equations of conservation laws. The new method has several advantages. First, it can solve deterministic conservation laws with discontinuous flux functions without large numerical errors, thus demonstrating that the proposed scheme achieves perfect numerical accuracy in the treatment of discontinuity in the flux functions. Second, it can compute the numerical flux corresponding to the real state of solution without relying on Riemann problem solvers. Third, reasonable accuracy can be obtained easily and no special treatment is needed for the numerical solution of the stochastic differential equations, because it is performed automatically in the integrated numerical flux function. Finally, the proposed approach does not require either nonlinear solvers or direct statistical approaches. Furthermore, it has strong applicability to various scalar conservation laws with stochastic time-space dependent flux functions as shown in

the numerical results.

The proposed finite volume Runge-Kutta method has been tested on stochastic Burgers equation, stochastic problems in traffic flow and two-phase flow applications. The obtained results indicate good shock resolution with high accuracy in smooth regions and without any nonphysical oscillations near the shock areas. The convergence to the correct steady-state solution has been clearly verified in a deterministic scalar conservation law with discontinuous flux function. Results presented in this paper have show high resolution of the proposed finite volume method and confirm its capability to provide accurate and efficient simulations for scalar conservation laws with stochastic time-space dependent flux functions. Future work will concentrate on extending the proposed method to hyperbolic systems of conservation laws with stochastic time-space dependent flux function in one and two space dimensions. Furthermore, since the difficulties arising from coefficients with multiplicative noise would not fit into the frame of this paper, we will only deal with stochastic conservation laws involving multiplicative noise in a forthcoming paper.

Acknowledgment. This work was partly performed while the second author was a visiting professor at department of mathematics, university of Taibah at Madinah. M. Seaid is deeply grateful to the Taibah university for their hospitality during a research visit there.

References

- [1] B. Andreianov, K. Karlsen, N. Risebro, A theory of L1-dissipative solvers for scalar conservation laws with discontinuous flux, *Archive Rat. Mech. Anal.* 201 (2011) 27–86.
- [2] C. Archubi, L. Braunstein, R. Buceta, Growing interfaces in quenched media: stochastic differential equation, *Physica A: Statistical Mechanics and its Applications* 283 (2000) 204–207.
- [3] I. Bonzani, L. Mussone, Stochastic modelling of traffic flow, *Mathematical and Computer Modelling* 36 (2002) 109–119.
- [4] A. Debussche, J. Vovelle, Scalar conservation laws with stochastic forcing, *Journal of Functional Analysis* 259 (2010) 1014–1042.
- [5] P. Degond, C. Ringhofer, Stochastic dynamics of long supply chains with random breakdowns, *SIAM J. Appl. Anal.* 68 (2007) 59–79.
- [6] S. Diehl, A conservation law with point source and discontinuous flux function, *SIAM J. Math. Anal.* 56 (1996) 388–419.
- [7] J. Feng, D. Nualart, Stochastic scalar conservation laws, *J. Funct. Anal.* 255 (2008) 313–373.

- [8] S. Frank, W. Schmickler, Ion transfer across liquidliquid interfaces from transition-state theory and stochastic molecular dynamics simulations, *J. Electroanalytical Chemistry* 590 (2006) 138–144.
- [9] R. Ghanem, P. Spanos, *Stochastic Finite Elements: A Spectral Approach*, Springer-Verlag, New York, 1991.
- [10] T. Gimse, N. Risebro, Solution of Cauchy problem for a conservation law with a discontinuous flux function, *SIAM J. Math. Anal.* 23 (1992) 635–648.
- [11] D. Gottlieb, D. Xiu, Galerkin method for wave equations with uncertain coefficients, *Comm. Comput. Phys.* 3 (2008) 505–518.
- [12] S. Heinz, *Statistical Mechanics of Turbulent Flows*, Springer-Verlag, Berlin, 2003.
- [13] H. Holden, N. Risebro, On the stochastic Buckley-Leverett equation, *SIAM J. Appl. Math.* 51 (1991) 1472–1488.
- [14] H. Holden, N. Risebro, A stochastic approach to conservation laws, In: *Third International Conference on Hyperbolic Problems. Theory, Numerical Methods and Applications*, Uppsala Eds. B. Engquist, B. Gustafsson (1991) 575–587.
- [15] H. Holden, N. Risebro, A mathematical model of traffic flow on a network of unidirectional roads, *SIAM J. Math. Anal.* 26 (1995) 999–1017.
- [16] H. Holden, N. Risebro, Conservation laws with a random source, *Appl. Math. Optim.* 36 (1997) 229–241.
- [17] H. Holden, B. Øksendal, J. Ubøe, T. Zhang, *Stochastic Partial Differential Equations: A Modeling, White Noise Functional Approach*, Springer-Verlag, 1996.
- [18] L. Holden, The Buckley-Leverett equation with spatially stochastic flux function, *SIAM J. Appl. Anal.* 57 (1997) 1443–1454.
- [19] T. Hou, W. Luo, B. Rozovski, H. Zhou, Wiener chaos expansions and numerical solutions of randomly forced equations of fluid mechanics, *J. Comput. Physics.* 216 (2006) 687–706.
- [20] J. Hurtado, A. Barbat, Monte Carlo techniques in computational stochastic mechanics, *Arch. Comput. Methods Engrg.* 5 (1998) 3–29.
- [21] E. Isaacson, B. Temple, Analysis of a singular hyperbolic system of conservation laws, *J. Diff. Equations.* 65 (1986) 250–268.
- [22] A. Jazwinski, *Stochastic Processes and Filtering Theory*, Academic Press, New York, 1970.
- [23] P. Jenny, M. Torrilhon, S. Heinz, A solution algorithm for the fluid dynamic equations based on a stochastic model for molecular motion, *J. Comput. Physics.* 229 (2010) 1077–1098.

- [24] M. Kaminski, Stochastic boundary element method analysis of the interface defects in composite materials, *Composite Structures* 94 (2012) 394–402.
- [25] K. Karlsen, C. Klingenberg, N. Risebro, A relaxation scheme for conservation laws with a discontinuous coefficient, *Math. Comp.* 73 (2003) 1235–1259.
- [26] P. Kloeden, E. Platen, *The Numerical Solution of Stochastic Differential Equations*, Springer Verlag, Berlin, 1999.
- [27] B. V. Leer, Towards the ultimate conservative difference schemes v. a second-order sequal to Godunov’s method, *J. Comp. Phys.* 32 (1979) 101–136.
- [28] M. Lighthill, J. Whitham, On kinematic waves: II. a theory of traffic flow on long crowded roads, *Proc. Royal. Soc. London, Series A.* 229 (1955) 317–345.
- [29] H. Manouzi, M. Seaïd, M. Zahri, Wick-stochastic finite element solution of reaction-diffusion problems, *J. Comp. Applied Math.* 203 (2007) 516–532.
- [30] K. Mohamed, Simulation numérique en volume finis, de problèmes d’écoulements multidimensionnels raides, par un schéma de flux á deux pas, Dissertation, University of Paris 13, 2005.
- [31] S. Osher, R. Fedkiw, *Level Set Methods and Dynamic Implicit Surfaces*, Springer-Verlag, Berlin, 2003.
- [32] G. Poëtte, B. Després, D. Lucor, Uncertainty quantification for systems of conservation laws, *J. Comp. Phys.* 228 (2009) 2443–2467.
- [33] J. L. Randall, *Numerical Methods for Conservation Laws, Lectures in Mathematics ETH Zürich*, 1992.
- [34] P. Roe, Approximate riemann solvers, parameter vectors and difference schemes, *J. Comp. Physics.* 43 (1981) 357–372.
- [35] A. Rößler, Rooted tree analysis for order conditions of stochastic Runge-Kutta methods for the weak approximation of stochastic differential equations, *Stochastic Anal. Appl.* 24 (2006) 97–134.
- [36] A. Rößler, Runge-Kutta methods for I t \hat{o} stochastic differential equations with scalar noise, *BIT* 46 (2006) 97–110.
- [37] A. Rößler, Second order Runge-Kutta methods for It \hat{o} stochastic differential equations, *SIAM J. Numer. Anal.* 47 (2009) 1713–1738.
- [38] V. Rusanov, Calculation of interaction of non-steady shock waves with obstacles, *J. Comp. Math. Phys. USSR* 1 (1961) 267–279.
- [39] M. Seaïd, Stable numerical methods for conservation laws with discontinuous flux function, *Appl. Math. Comput.* 175 (2006) 383–400.
- [40] M. Serrano, K. Klemm, F. Vazquez, V. Eguíluz, M. S. Miguel, Conservation laws for voter-like models on random directed networks, *J. Stat. Mech.* 2009 (2009) P10024.

- [41] A. Sopasakis, Stochastic noise approach to traffic flow modeling, *Physica A* 342 (2004) 741–754.
- [42] P. Sweby, High resolution schemes using flux limiters for hyperbolic conservation laws, *SIAM J. Numer. Anal.* 21 (1984) 995–1011.
- [43] T. Tang, T. Zhou, Convergence analysis for stochastic collocation methods to scalar hyperbolic equations with a random wave speed, *Commun. Comput. Phys.* 8 (2010) 226–248.
- [44] J. Tryoen, O. L. Maitre, A. Ern, Adaptive anisotropic spectral stochastic methods for uncertain scalar conservation laws, *SIAM J. Sci. Comp.* To appear.
- [45] J. Tryoen, O. L. Maitre, M. Ndjinga, A. Ern, Roe solver with entropy corrector for uncertain hyperbolic systems, *J. Comput. App. Math.* 235 (2010) 491–506.
- [46] K. Waldeer, A numeric investigation of a vehicular traffic flow model based on a stochastic acceleration process, *Computer Physics Communications* 147 (2002) 650–653.
- [47] D. Yang, J. Zhang, Z. Lu, Stochastic analysis of saturated-unsaturated flow in heterogeneous media by combining Karhunen-Loeve expansion and perturbation method, *J. Hydrology.* 294 (2004) 18–38.
- [48] T. Zhou, Stochastic Galerkin methods for elliptic interface problems with random input, *J. Comput. App. Math.* 236 (2011) 782–792.
- [49] T. Zhou, T. Tang, Galerkin methods for stochastic hyperbolic problems using bi-orthogonal polynomials, *J. Sci. Comput.* 51 (2012) 274–292.